Journal Name

ARTICLE

Self-immobilized Pd nanowires as an excellent platform for a continuous flow reactor: Efficiency, stability and regeneration

33333333Received 00th January 20xx,
Accepted 00th January 20xx

DOI: 10.1039/x0xx00000x

www.rsc.org/

Lipipuspa Sahoo, [a‡] Moumita Rana, [b‡] Sanjit Mondal, [a] Neeru Mittal, [a] Pronoy Nandi,[c,d] A. Gloskovskii, [e] U. Manju,[f] D. Topwal,[c] Ujjal K Gautam[a*]

Despite extensive use of Pd nanocrystals as catalysts, the realization of a Pd based continuous flow reactor remains a challenge. Difficulties arise due to ill-defined anchoring of the nanocrystals on a substrate and reactivity of the substrate under different reaction conditions. We demonstrate the first metal (Pd) nanowire based catalytic flow reactor that can be used across different filtration platforms, wherein reactants flow through a porous network of nanowires (10-1000 nm pore-sizes) and the product can be collected as filtrate. Controlling the growth parameters and obtaining high aspect ratio of the nanowires (diameter= ~13 nm and length>8000 nm) is necessary for successful fabrication of this flow reactor. The reactor performance is similar to a conventional reactor, but without requiring energy expensive mechanical stirring. Synchrotron based EXAFS studies were used to examine the catalyst microstructure and *Operando* FT-IR spectroscopic studies were used to device a regenerative strategy. We show that after prolonged use, the catalyst performance can be regenerated up to 99% by a simple wash-off process without disturbing the catalyst bed. Thus collecting, regenerating and redispersing processes of the catalyst in the conventional industrial reactors can be avoided. Another important advantage is avoiding specific catalyst anchoring substrates, which are not only expensive, but also not-universal in nature.

Introduction

Use of heterogeneous metal catalysts has facilitated the synthesis of many industrially important chemicals. Nanostructuring of metals improves their catalytic activity significantly by enhancing their surface to volume ratio and tuning the electronic property.[1] Thus investigations on organic transformation reaction using noble metal nanoparticles are gaining enormous attention during the last decade.[2-5] Among the noble metals, the role of Pd is particularly important due to its use in several key organic transformations such as oxidative homocoupling reactions, cross-coupling reactions, hydrogenation reactions and nitro group reduction reactions.[3-9]

While constituting larger scale reactors, the affordable recovery and recycling of the nanocrystalline metal catalysts from the reaction mixture, besides their efficiency, has emerged as a key industrial concern. Freely floating catalyst nanocrystals in a reactor require constant mechanical agitation to maintain a homogeneous dispersion, else their tendency for agglomeration and precipitation leads to significant reduction in active surface area.[10] This has inspired investigations in constructing lab-scale continuous flow reactors that potentially allows flow of reactant molecules over immobilized catalyst nanocrystals, thereby avoiding the needs for catalyst dispersion and separation from reaction medium.[11-15] Immobilization requires the catalyst particles to be strongly anchored on a catalyst support. Researchers have employed various kinds of materials as supports, including various types of amyloids, polymers, cotton fabrics, and even magnetic colloidal particles.[11,16-18] However a common problem is encountered in these approaches of ex-situ generation of nanoparticle and further combining them with the support, when nanoparticles form super-lattices or random agglomeration, thereby decreasing the overall active surface.[19,20] In addition, if the interaction between nanoparticles and the support is not uniformly and sufficiently strong, the particles gradually leaches out during reaction processes.[21] Loading of nanoparticles on support also undesirably leads to masking of a significant portion of catalyst surface area.[22,23] Due to such factors, catalyst activity in a flow reactor suffers from irrecoverable losses.

Use of the catalysts without a support is preferable when the support has high cost, low stability at higher temperature and poor usability across different solvents. Since the supports themselves cannot make a reactor bed for continuous flow reactors, it is required to coat these on solid porous membranes. Porosity determines the retention time of reactants and catalytic efficiency. The widely used nanoporous membranes obtained from nitrocellulose, PVDF, PTFE etc. needs high pressure to facilitate speedy permeation of the

a Department of Chemical Sciences, Indian Institute of Science Education and Research (IISER)-Mohali, Sector 81, Mohali, SAS Nagar, Punjab 140306, India
b IMDEA Materials Institute, C/Eric Kandel 2, Parque de Tecnogetafe, Getafe -28906, Spain
c Institute of Physics, Sachivalaya Marg, Bhubaneswar - 751005, India
d Homi Bhabha National Institute, Training School Complex, Anushakti Nagar, Mumbai - 400085, India
e DESY Photon Science, Deutsches Elektronen-Synchrotron, 22603 Hamburg, Germany
f CSIR -Institute of Minerals and Materials Technology, Bhubaneswar - 751013, India

Journal Name

ARTICLE

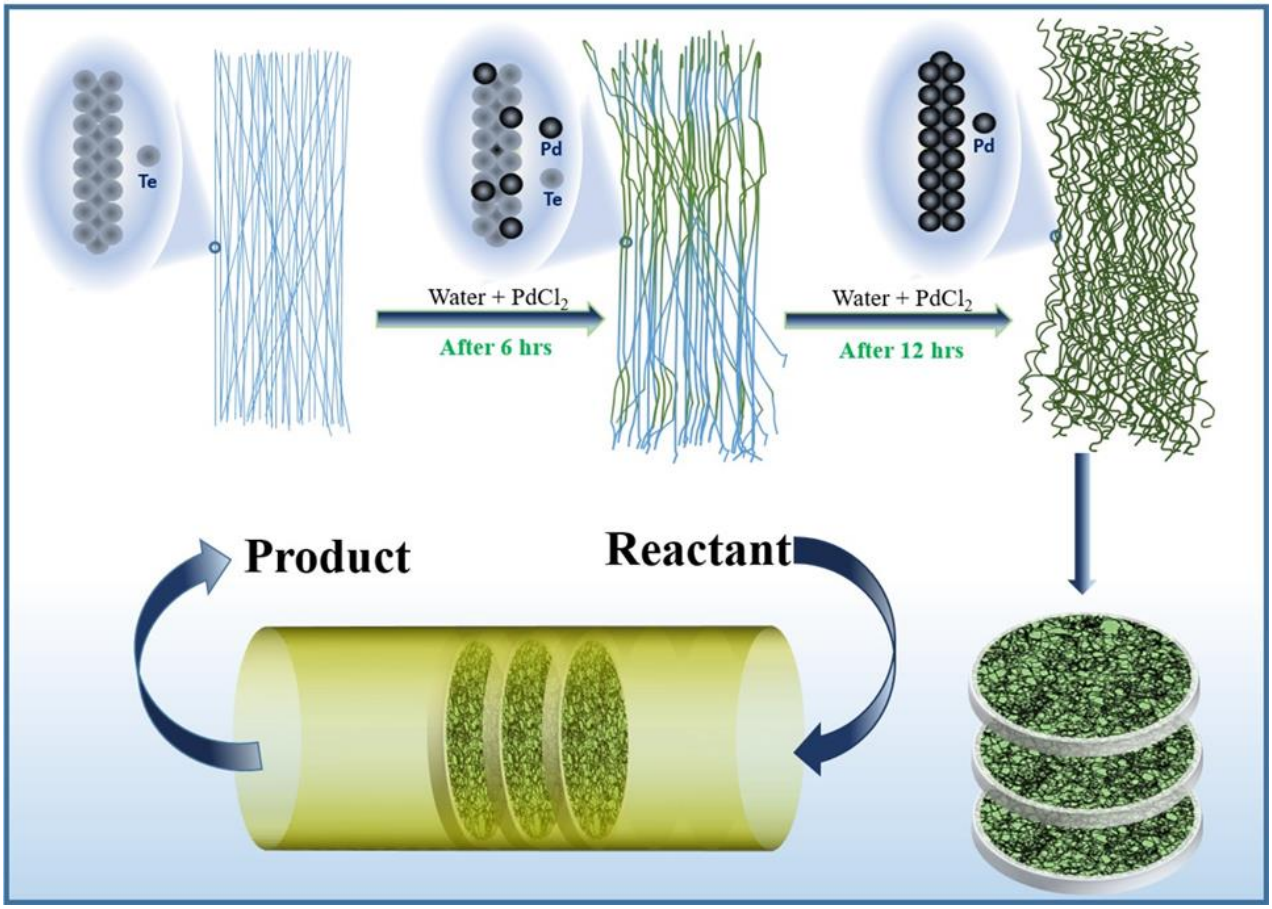

Fig. 1 Schematic illustration of a proposed flow reactor. Galvanic displacement of straight and very long Te NWs yields Pd NWs that are not-so-straight and easily self-entangle. Therefore, these NWs cannot pass through during filtration. Instead, they stick onto the surface of the filtration bed, even without requiring a specific NW-filtration-bed interaction, forming a network having tiny pores. Reactants of a Pd catalyzed reaction can pass across this flow reactor, yielding products at the outlet.

reactant molecules.[11,13,24-26] On the other hand, rapid mass flow of reactants can be achieved using membranes with larger pores like microporous alumina membrane, silica monoliths, ceramic membrane etc., but often with incomplete conversion due to insufficient reactant-catalyst contact, unless large amounts of catalysts used.[14,15,27,28] Therefore it is deemed vastly advantageous to achieve higher throughput at atmospheric pressure, by tailoring porosity and avoiding catalyst supports. Recently, Koga *et al*. demonstrated a promising microporous paper-based continuous flow reactor, though recovery of the implanted nanocatalysts with a strong catalyst support interaction is extremely difficult and may even require disassembling the reactor.[15]

It occurred to us that if the nanocrystals themselves can organize to create a robust network of small pores with highly exposed surface area, it can directly be mounted on a solid porous membrane and the use of catalyst support can be avoided. In this context, it may be pointed out that in one of our recent studies, while developing Pt-based nanowires for electrocatalytic applications, we reported observing the nanowires forming porous films (pore sizes ranging from few to few hundred nanometers) with high mechanical stability due to extensive self-entanglement.[29] This led us to hypothesize that if catalyst NWs with length sufficiently higher than the membrane pore-size is obtained, and a solution of the same is made to pass across the membrane, the NWs will be retained on the membrane surface forming a thin porous film even in absence of a strong NW-membrane interaction (Fig. 1). This can be the basis of an affordable flow reactor that would work on any type of membrane. If the wires are not straight, the NW-NW contact

area would be minimal, exposing almost entire surface to the reactants. In addition, the absence of chemical interaction will help in simple recovery of the catalysts. At this point the challenge would be the regeneration of the catalyst bed without disturbing the reactor arrangement.[14,30]

Here we demonstrate configuring a continuous-flow column reactor using Pd NW membrane mounted on filtration bed when using reduction of p-nitrophenol (4NP) to p-aminophenol (4AP) by $NaBH_4$ as a model reaction. Pd Nanowires (NWs) with very high aspect ratio were synthesized by galvanic displacement method using Te nanowires as the sacrificial template. The Pd nanowires have shown notable catalytic activity with a rate constant of ~0.02 s^{-1} for 4NP reduction, superior to many of the state-of-the-art catalysts. The continuous-flow column reactor fabricated using these NWs has shown ~100% conversion efficiency for several batches of the reaction mixtures, before started to decline. Operando IR spectroscopy was used to examine the origin of declining activity which established the generation of a boron species in the solution phase which subsequently gets adsorbed on the

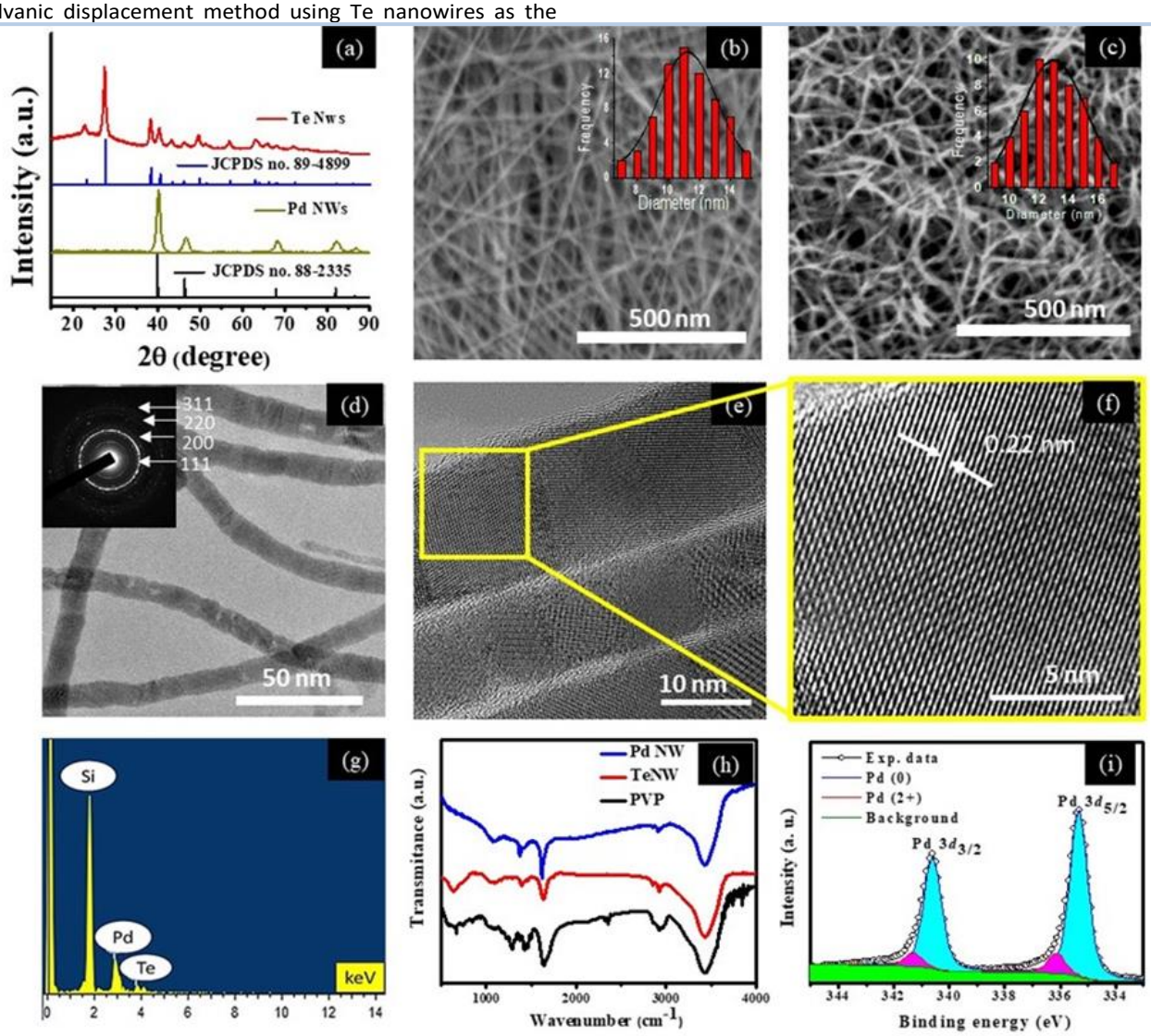

Fig. 2 (a) Powder XRD patterns of the Te and Pd NWs respectively. Expected peak positions for the pure phases are also depicted. (b, c) SEM images of Te and Pd NWs respectively. Insets show the respective distribution of the NW diameter. (d) TEM image of Pd NWs. Inset shows the corresponding SAED pattern (e, f) High-resolution TEM images of Pd NWs. (g) Representative EDS spectrum of Pd NWs showing the presence of a tiny amount of Te. (h) FTIR spectra of PVP, Te NWs, Pd NWs. (i) HAXPES spectrum of Pd 3d acquired on as-obtained NWs.

catalyst surface. A wash-off strategy was developed to regenerate original activity of the catalyst bed without disturbing it. The catalyst bed was found to be highly durable; with no change in catalyst morphology after 20 batches of reaction. Simple fabrication, high efficiency and easy catalyst recyclability make such a columnar flow reactor promising for Pd catalyzed reactions.

Results and discussion

In order to make a catalytic flow-reactor, as described in Fig. 1, we first generated Pd NWs with high aspect ratios by employing

a galvanic displacement approach wherein Te NWs were used as the sacrificial template. Synthesis of very high aspect ratio metal nanowires, in general, is difficult in absence of a structure directing template due to their isotopic growth habits, which can be altered to some extent by using shape directing agents.[31-34] Phase pure Te NWs were synthesized hydrothermally by reacting Na_2TeO_3, hydrazine hydrate and aqueous ammonia solution in presence of PVP (Fig. 2a). Electron microscopy images (Fig. 2b) show straight Te NWs with very high aspect ratios, with average diameters of ~11 nm with narrow diameter distribution (inset of Fig. 2b) and lengths ranging from 8-10 µm (Fig. S1). Further to prepare Pd NWs, Te NWs were precipitated with acetone to get rid of excess the hydrazine and ammonia. These were then dispersed in water and $PdCl_2$ solution was added and kept in an incubator at 30 °C for 12 h. The higher reduction potential of Pd facilitated the galvanic displacement of Te from the NWs, when Te gradually dissolved away as TeO_3^{2-} while reduced Pd2+ deposited on the NWs in the following manner:

$$Te + 2PdCl_2 + 3H_2O \longrightarrow TeO_3^{2-} + 2Pd + 4Cl^- + 6H^+$$

(Pd^{2+}/Pd, $E^o = 0.95$ V and Te^{4+}/Te, $E^o = 0.60$ V)

The Powder X-ray diffraction (PXRD) pattern of the product revealed that the NWs have face centered cubic phase (FCC) (180870-ICSD) of Pd (Fig. 2a). The broadening of the diffraction peaks suggests that Pd is in nanodimension. Structural features were further examined using electron microscope. SEM and TEM images confirmed the presence of Pd nanowires only, and no other morphology (Fig. 2c-f). The mean diameter of Pd NWs was found to be ~13 nm with a narrow diameter distribution (Inset of Fig. 2c) and length ~8-10 µm, similar to that of precursor Te NWs (Fig. S2). One can clearly observe in the images that these NWs get entangled during deposition to form network of nanowires. As we pointed out previously, similar Pd NWs can form free-standing and robust porous membrane upon drop casting due to high aspect ratio and 'non-straight' nature.[29] In order to check microstructure of the Pd NWs, high resolution TEM (HRTEM) images were recorded. Fig. 2f is a typical HRTEM image of the NWs showing distinct lattice fringes with d spacing of 0.22 nm corresponding to [111] lattice planes of Pd. Importantly, HRTEM images and SAED patterns (inset in Fig. 2d) also confirmed that the NWs are polycrystalline in nature and thereby inducing 'bends' in the otherwise straight Te nanowires. To determine the extent of galvanic displacement, the nanowires were analyzed using Energy Dispersive X-ray (EDS) spectroscopy (Fig. 2g) and ICP-OES which indicated presence of about 7-10% of Te. The Te fraction is amorphous as no diffraction peak was observed in diffraction studies. The presence of PVP in the NWs was confirmed from Fourier transformed infrared (FTIR) spectra of the samples. As seen in Fig. 2h, a peak at 1633 cm^{-1} corresponding to C=O stretching and peaks at 2938 cm^{-1} and 2869 cm^{-1} corresponding to $-CH_2$ stretching of PVP are present in both the Te and the Pd NWs.[35]

In regards to maintaining the high aspect ratio of the Te NW template, which is essential for the flow reactor design, it is important to note that usual galvanic displacement in aqueous medium results in Pd nanoparticles (NPs) due to faster reaction kinetics.[36] On the other hand, even though NWs have been isolated from aqueous medium, these reports do not compare the lengths of parent Te and the Pd NWs, which in our experience may be different.[37,38] As discussed in detail in Supporting Information, we found it absolutely necessary to remove trace amount of ammonia left over from the Te NW synthesis step, which otherwise changes the pH of the solution and makes the displacement kinetics faster leading to fragmentation of the Te NWs (Fig. S3).

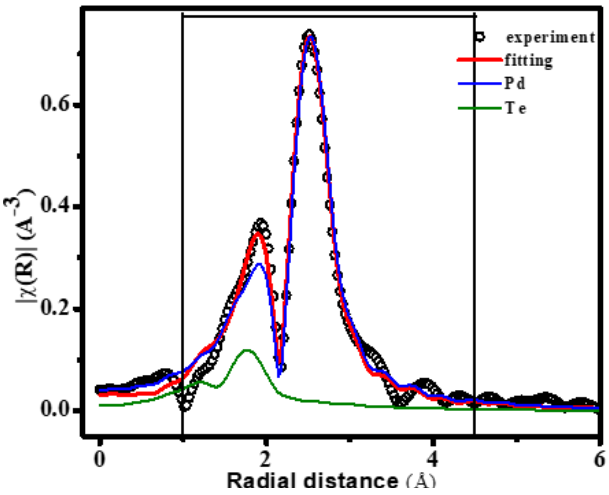

Fig. 3 Fourier transform of k^2 weighted EXAFS data ($|\chi(R)|$) at Pd K edge, along with corresponding fittings (contribution from Pd, Te and overall) superimposed on it.

HAXPES, EXAFS studies and identification of a possible Pd-Te phase: Electronic structure of Pd NWs was investigated using Hard X-ray photoelectron spectroscopy (HAXPES) measurements. Core level photoemission spectra acquired at the Pd 3d level (shown in Fig. (2i)) consists predominantly of doublets arising from the spin-orbit split Pd $3d_{5/2}$ and $3d_{3/2}$ components appearing at 335.3 eV and 340.6 eV binding energies, respectively, corresponding to Pd(0) state.[38] A careful spectral decomposition of the 3d spectra also shows the appearance of another set of spin-orbit split components appearing at higher binding energies, 336.1 eV and 341.4 eV, which may be corresponding to the Pd 3d components originating from surface oxidation of Pd.[39]

Use of a Te template is the only method to obtain Pd nanowires with very high aspect ratios and this has been extensively used. Pd nanowires and nanorods can be obtained in the absence of a template also. But the length of the nanowires is much smaller and not suitable for self-entanglement and formation of a flow reactor. It is to be noted that a number of Pd-Te phases are known and since in the galvanic process such as the one we have employed, both Te and Pd species undergo changes in oxidation state associated with mutual electron transfer, there

Table 1. Pd K-edge EXAFS data analysis for the Pd NWs

Single Scattering path	N	R(Å)	σ^2 (Å^2)
Pd-Pd	10.915	2.7738	0.01541
Pd-Te	1.085	2.6265	0.01541

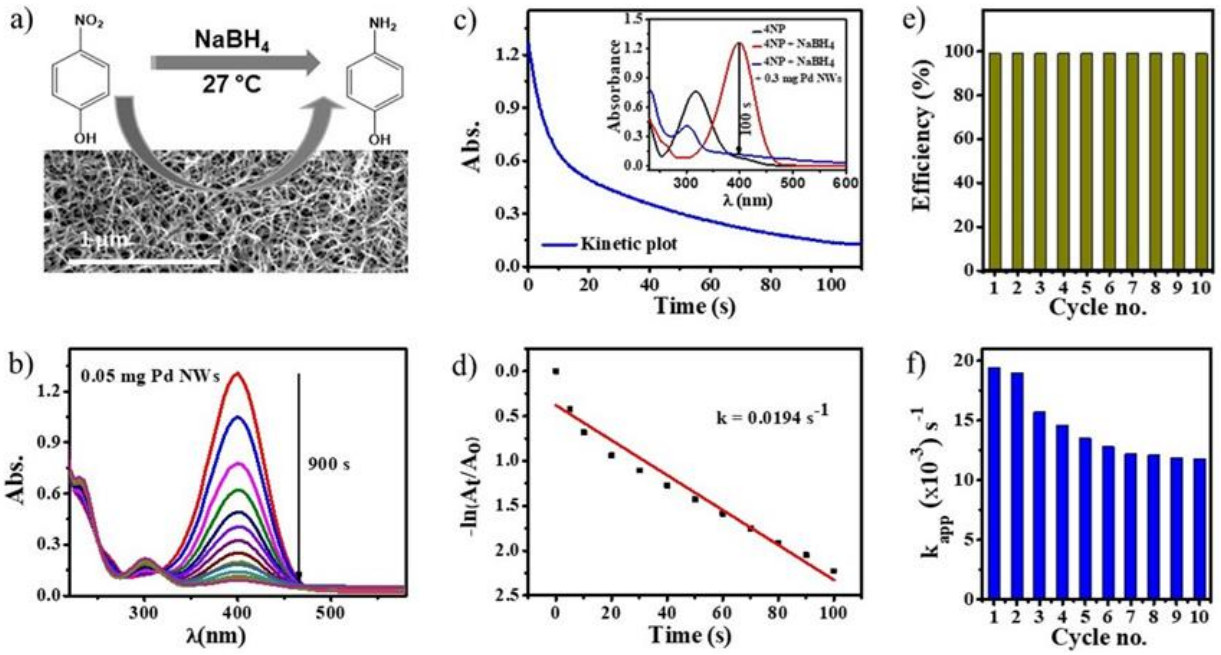

Fig. 4 4NP reduction reaction using Pd NWs: (a) schematic representation, (b) time-dependent UV-Vis absorption spectra of the reaction solution using 0.05 mg of Pd NWs (c) Kinetic data monitored at 400 nm while using 0.3 mg Pd NWs (inset: corresponding UV-Vis absorption spectra), (d) corresponding plot of ln(At/A0) versus time for 4NP reduction. (e) Conversion efficiency plot and (f) the corresponding rate constant plots for 10 catalytic cycles.

is a possibility of formation of a tiny quantity of Pd-Te phase.In order to investigate further the interaction between Pd and Te in the nanowires, Extended X-ray Absorption Fine Structure (EXAFS) measurements were performed on the NWs. Fig. 3 represents the magnitude of Fourier transform of k2 weighted EXAFS data (|χ(R)|) at Pd K edge, along with corresponding fittings (contribution from Pd, Te and overall) superimposed on it. Fitting of experimental data was confined to the k range of 3 < k < 11 Å-1 and R range of 1.2 < R < 4 Å and all the fitting parameters including coordination number, bond length, mean square relative displacement are presented in Table 1. Relatively low R factor~ 0.0092 corroborates small distortion in the sample. In Fig. 3 second shell (~2.5 Å) can be attributed to metallic Pd-Pd coordination with FCC lattice, [40,41] whereas the first shell (~1.9 Å) matches well with the fitting for Pd-Te phase (8.94%) revealing the existence of a Pd-Te phase in Pd NWs.[42]

Reduction of p-nitrophenol to p-aminophenol: To evaluate the catalytic performance of the Pd nanowires (NWs), hydrogenation of 4-Nitrophenol (4NP) by $NaBH_4$ was performed as the model reaction (Fig. 4a).[43,44] The reaction kinetics was monitored by analyzing the absorption spectrum of 4NP, which gives a characteristic strong peak at 400 nm in presence of $NaBH_4$ (pH>12) due to formation of 4-Nitrophenolate ion.[45] We confirmed that the reaction does not take place in absence of the catalyst even if kept for a week. Although the thermodynamic reduction potential of the reactants (H_3BO_3/BH_4^- = -1.33 V) and 4NP/4AP = 0.76 V, versus NHE) suggests that the reduction of 4NP is thermodynamically feasible, the reaction is kinetically extremely slow. However, it can be quickly initiated by a catalyst. Upon addition of our Pd NWs, the peak at 400 nm gradually lowered in intensity and the peak corresponding to 4AP at 298 nm intensified (Fig. 4b). We used large excess of $NaBH_4$ to ensure that the reaction rate does not alter with minute changes in its concentration and the reaction kinetics can be assumed to be pseudo first-order with respect to 4NP concentration. Catalysis was performed using different amounts of catalyst. UV-Vis spectra of 4NP reduction reaction after addition of 0.05 mg of Pd NWs are shown in Fig. 4b which exhibit an isosbestic point indicating that no other reaction product formed. The reaction completed within 100 seconds of initiation (Fig. 4c) when 0.3 mg of catalyst was used (inset of Fig. 4c shows the corresponding spectra). Assuming the reaction to follow a 1st order kinetics, the rate constant was calculated to be 0.0194 s^{-1} (Fig. 4d). To perform the recyclability test, the NWs were again collected by centrifugation after the 1st catalysis test and used for the second set of reaction under identical conditions without addition of any more NW catalyst. The reaction was found to be 100% complete each time for 10 consecutive cycles (Fig. 4e). However, the time required for the completion of the reaction increased with every cycle (Fig. 4f). The rate constants estimated for each cycle are tabulated in Table S1. There was nearly 2% (k=0.0190 s^{-1}) and 17% (k=0.0157 s^{-1}) activity loss at the end of second and third cycle respectively. At the end of the tenth cycle, there was 40% lowering of catalyst activity (k=0.0118 s^{-1}). It may be noted that even though the activity of these NWs was not expected to be as high as other reported Pd particles initially, owing to their lesser geometric surface area, the time taken for complete conversion of 4NP

Journal Name

ARTICLE

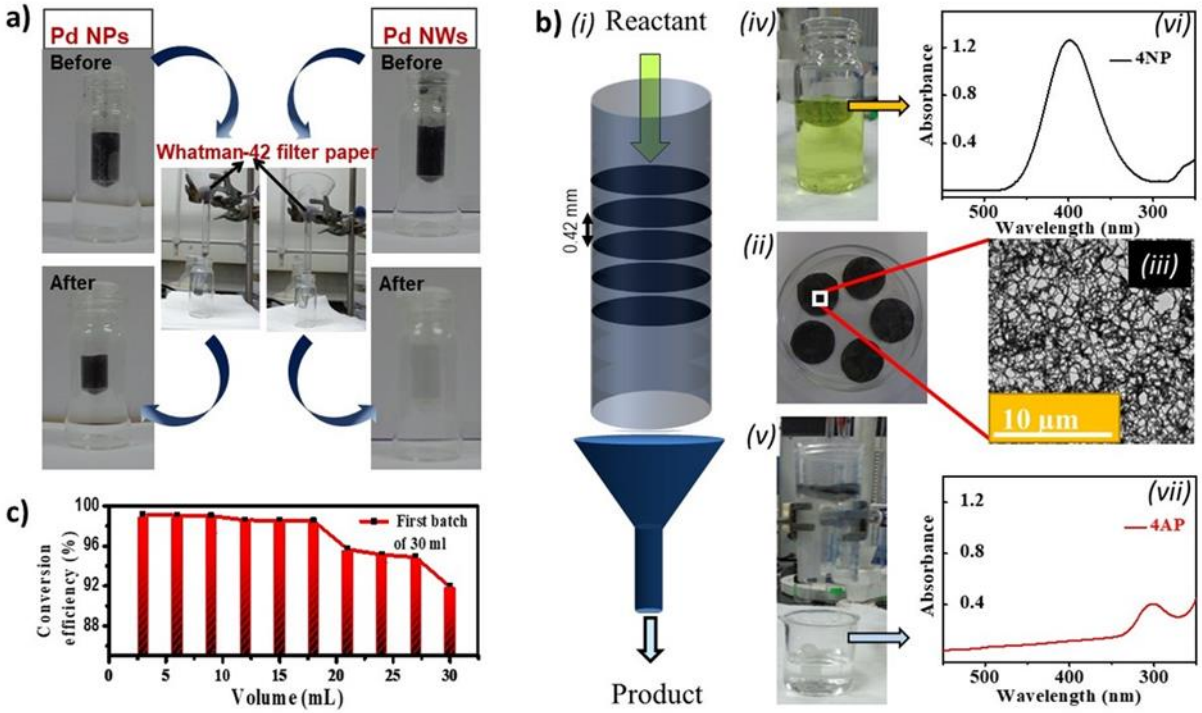

Fig. 5 (a) Illustration of filtration of Pd NPs and Pd NWs over Whatman 42 filter paper. While the NPs easily pass through the filter paper, the NWs firmly stick to the filter paper due to self-entanglement. b) Continuous flow reactor set-up fabricated in lab: (i) schematic presentation, (ii) catalyst loaded filter papers, (iii) SEM images of the NWs on filter paper, (iv) the reactant mixture, (v) experimental set-up, (vi, vii) UV-Vis spectra of the reaction mixture before and after passing through the reactor.

(and turnover frequency, TOF) is at par with many of the superior catalysts reported in literature recently (Table S2). Possible reasons for the decrease in the activity as the number of cycle proceeds may be due to surface restructuring of the Pd NWs or poisoning of active sites or partly due to loss of Pd NWs after every cycle during the process of catalyst washing. SEM images of the nanowires after catalysis showed that there was no noticeable change in their morphology (Fig. S8).

Design of a flow reactor: The very high aspect ratio of the Pd NWs makes them distinct from others' catalysts during filtration. Fig. 5a compares the filtration of Pd nanowires with nanoparticles. As seen, when a dispersion of a Pd nanoparticles is poured onto a medium-speed Whatman-42 paper, the entire content flow down the funnel. The NWs, on the other hand, are too long for the 2.5 µm filtration pores and gets retained on the paper surface. Length and the 'not-straight' nature of the NWs seem to actually make them behave like a lock of untidy hair leading to self-entanglement, and this led to the possibility of designing of a catalyst bed on a filtration platform. Similar entanglement was observed while drying the samples for SEM too, creating 10-1000 nanometer holes (Fig. S9). In this context, it can be hypothesized that if reactants are made to flow vertically through such beds, these will easily interact with the catalyst surface and the product formed could be collected at the outlet. Since the pores are rather small, the situation can be compared with very high concentration of catalysts which will not only lead to enhanced reaction rate, but also help avoiding mechanical mixing or stirring of the solution. In order to make a catalyst bed, we first prepared a catalyst ink using 5 mg of the Pd NWs dispersed in 5 ml of ethanol, which was uniformly drop-casted onto a 3 cm diameter Whatman-42 paper and dried naturally. The entangled Pd NWs formed a film on the surface of the filter paper and the paper appeared black. Five such catalyst beds were then loaded on a plastic cylinder as shown in Fig. 5b (i & ii) to make the flow reactor. SEM image of the nanowires decorating the filter paper is shown in the Fig. 5b (iii). The pores created by entangled NWs ranges from a few to

Journal Name

ARTICLE

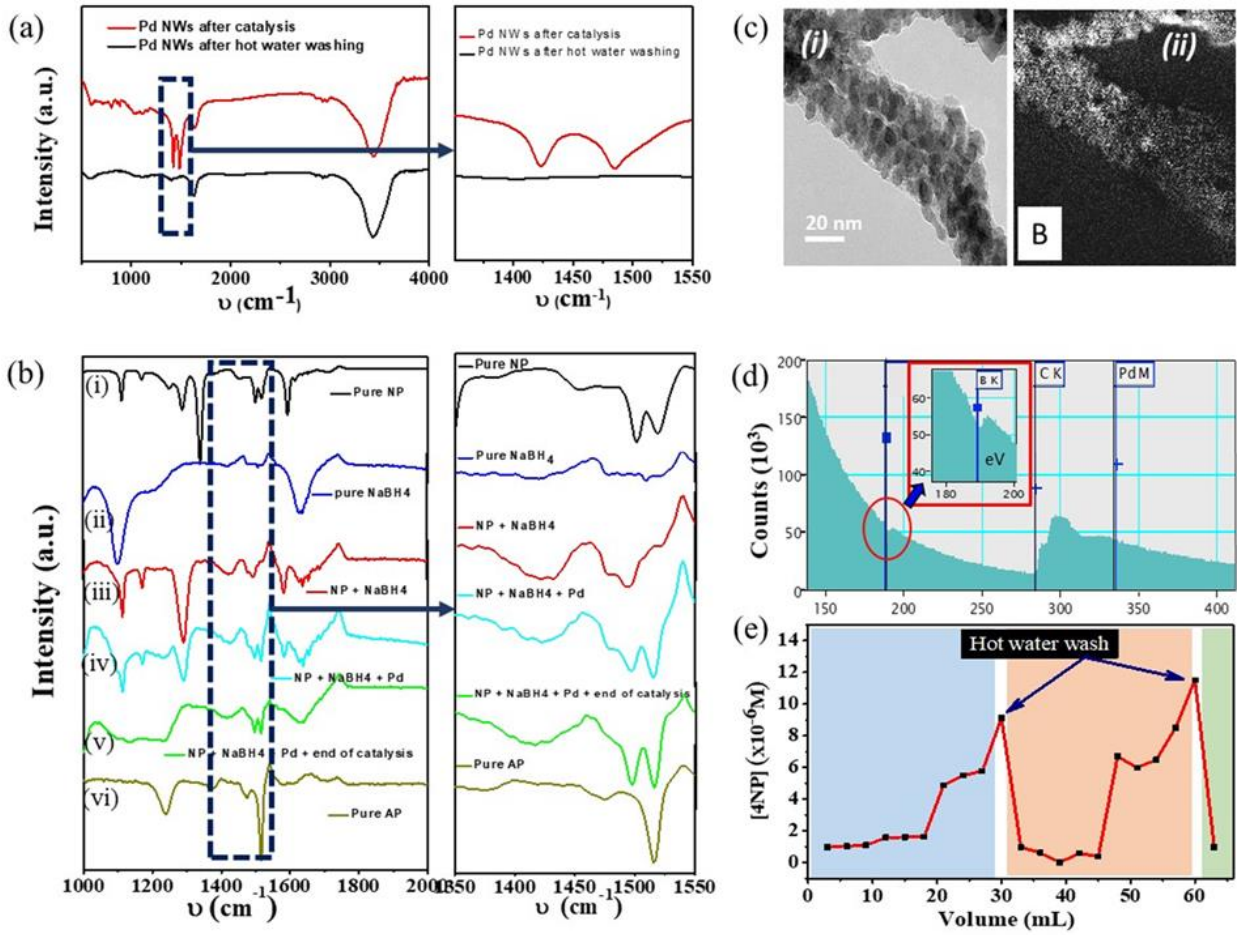

Fig. 6. (a) FTIR spectra of the Pd NWs after catalysis and after hot water washing. (b) In-situ FTIR spectra acquired during catalysis for all the reactants and products, (c) (i) TEM image and (ii) EFTEM mapping image of B on NWs, (d) EELS spectrum of Pd NWs after catalysis, (e) concentration of 4NP in the product after each batch (3 ml) of reactants passing through the flow reactor. The plot also depicts regeneration catalyst activity after hot water washing.

few hundreds of nanometer, much smaller than those in the filter paper. In order to test the efficiency of the reactor, 3 ml of the reaction mixture consisting of 4NP and $NaBH_4$ was allowed to flow through it at a rate of 6 ml/min. The flow rate was optimized with a blank experiment by making water to flow through the catalyst beds. Once the reactants were introduced, the progress of the reaction was monitored by collecting the absorption spectra of the filtrate periodically. The filtrate appeared colorless and the peaks corresponding to the 4NP completely disappeared, confirming 100% conversion of 4NP (Fig. 5b (iv-vii). Thereafter, we continued to add batches of 3 ml reaction mixture in successive steps and analyzed the concentration of 4NP in the filtrate. The results of the batch experiments are shown in Fig. 5c. After addition of 18 mL of the reaction mixture, the concentration of 4NP in the product was found to be 1.7 times than that when 3 mL was added (>98% conversion). Performance started to reduce gradually and by the time a total of 30 mL reactant was added (10^{th} batch), the extent of conversion came down to about 92% due to catalyst poisoning.

This brings forth a crucial factor in designing of the flow reactor. Many previous reports on 4NP reduction depicted decrease in catalytic efficiency even after 5^{th} cycle up to 30% of the initial activity.[30] On the other hand, even though many catalysts showed complete conversion even after 10th cycle, the time required for complete conversion was significantly longer which can be inferred from a gradual decrease in activity. In order to achieve efficient flow reactor set-up, it is necessary

to maintain a consistent flow rate of reactants i.e. same residual contact time between the reactants and the surface of the catalyst. This would naturally lead to lower conversion with catalyst deactivation and therefore its surface has to be regenerated at regular intervals.[14] However nothing much could be found about the origin of activity degradation during nitrophenol reduction in presence of $NaBH_4$, even though catalyst washing under sonication is near ubiquitously employed (but cannot be implemented for the current procedure). We therefore further investigated the origin of catalyst deactivation using operando infrared spectroscopy to develop a regeneration strategy. It should be accounted that operando spectroscopic studies have been previously carried out when nitroaromatics are being reduced by H_2 under high pressure.[46,47]

Fig. 6a compares the FTIR spectra acquired on the NWs before and after catalysis, indicating the presence of two additional peaks at 1425 and 1484 cm^{-1} in the used NWs. These peaks are different from normal NaBH4 degradation peaks in aqueous medium and not likely to be the B-O stretching and deformation frequencies appearing at 1350 cm^{-1} and 1241 cm^{-1} respectively.[48] Also, these peaks cannot be due to 4NP too, because even though 1484 cm^{-1} peak is close to C-H stretching, there should be an even stronger peak at 1342 cm^{-1} for N=O symmetric stretching. We also excluded the presence of 4AP on catalyst surface since the strong signature peak at 1242 cm^{-1} is entirely missing. Thus, the new peaks indicate the presence of a new species. Notably these are not related to PVP peaks in the catalyst NWs as well (*vide infra*), which repeatedly vanish with catalyst regeneration and reappears upon use.

To investigate further on the catalyst poisoning species, we have carried out in-situ IR spectroscopy during the reactions using a ATR IR setup. First we recorded spectrum for 4NP and $NaBH_4$ solution used in the flow reactor. As observed in Fig. 6b iii, a new peak appeared at 1418 cm^{-1} with an FWHM of about 40 cm^{-1} and continued to be there with time. Subsequently as we repeated the experiment using the same aliquot along with the catalyst NWs, when the same peak appeared again and continued to remain unaltered with progress of the reaction (Fig. S10). Interestingly, this new peak (at 1418 cm^{-1}) along with the sharp peaks (at 1425 and 1484 cm^{-1}) those appeared in the used NW Spectrum (*vide supra*, Fig. 6a) lies at the same position. Therefore, we believe that these peaks should be related and originated from the interaction of borohydride and 4NP in this instance and probably in any instance of 4NP reduction by $NaBH_4$ as well. Such a notion was further confirmed by using Pd nanoparticles as catalyst for the same reaction. IR spectrum of the used Pd NP catalyst showed similar peaks as that of used Pd NWs (Fig. S11). This catalyst poisoning species is X-ray amorphous as no discernible diffraction peak could be found in the XRD pattern of the used Pd catalysts. To confirm our assumption on the presence of B within this species, we have carried out elemental analysis (energy-filtered TEM mapping) on the used catalysts. Elemental mapping (Fig. 6c) and EELS spectrum (Fig. 6d) confirmed that this catalyst poisoning species contains boron and is uniformly distributed over the surface of used Pd NWs.

As the catalyst poisoning species is some compound of boron and forms a coating over the NWs, we presumed that it can be soluble to some extent in water and therefore could be washed off by a flow of water. We therefore poured few milliliters of hot water on the reactor (about 60-70 ^oC) and found that these two peaks indeed disappeared in the IR spectrum of the washed NWs and catalytic activity of the NWs were fully regained (on the contrary, cold water washing was not very effective). A second set of batch experiments were carried out under identical conditions using the regenerated flow reactor to check the efficiency of the regenerated catalysts as given in Fig. S12. As seen in Fig. 6e, the complete conversion of 4NP was observed for the first 5 batches. The catalyst-beds were further washed with hot water after the 10^{th} batch and activity was regained for the third time. To estimate the catalytic efficiency of the Pd NWs in flow reactor, we have compared the TOF of various recently reported flow reactor (Table S3). At high 4-NP conc. with a flow rate of 3 ml/min, we achieved conversion up to 90% with a TOF of 0.65 min^{-1} which is comparable to other reported catalyst.

Finally, recovery of expensive metals after catalysis has been a major challenge. The commonly adopted approach is to dissolve them in aqua regia and then to precipitate them by addition of a strong base.[15,49] These Pd NWs, on the other hand, are easily recoverable due to absence of strong interaction between filter paper and NWs, making the process more sustainable (Figure S13).

Conclusions

In conclusion, we have designed the first Pd based continuous flow reactor using its nanowires which can potentially be mounted on any filtration platform. We demonstrated that the reactant can be poured onto the catalyst loaded bed and the product can be obtained in the form of filtrate, thereby getting rid of the tedious and energy expensive mechanical mixing process. Similar flow reactor cannot be obtained using other nanostructures since most of these would pass through any filtration bed, and hence special anchoring procedure has to be formulated. Nanowires self-entangle creating a net that not only get stuck on the filtration bed, but also create holes as small as few nanometers, finer than any commercial filter. Using a model reaction of 4NP reduction, the reactor retained over 90% of efficiency after 10 batches of reactions at a constant flow-rate, which is superior to most state of the art catalysts tested under conventional procedure. We employed operando spectroscopic studies to identify the catalyst deactivating species, based on which a simple catalyst-regeneration strategy was developed without disturbing the reactor bed, and 100% efficiency was regained multiple times. This reactor, in principle, is highly propitious for other Pd catalyzed reactions as well and the strategy of using nanowires may lead to fabrication of very efficient flow reactors.

Experimental methods:

Chemicals: Sodium tellurite (Na_2TeO_3, 99.9%), Palladium (II) Chloride ($PdCl_2$, 99.9% Pd basis), Poly (vinyl pyrrolidone) (PVP average mol wt. 40,000), Hydrazine hydrate ($H_4N_2.H_2O$, 99%, AR), 4NP (99%), $NaBH_4$ (99%) were purchased from Sigma-Aldrich and aqueous ammonia solution (NH_3, about 30%, AR) was purchased from Himedia. All the chemicals were used as received without further purification. Ultrapure water with resistivity 18.2 MΩ was used for all the experiment.

Synthesis: Te NWs were first synthesized and used as template for synthesis of Pd NWs. Briefly, 1 g PVP (40k) and 0.0922 g Na_2TeO_3 (0.416 mmol) were dissolved in 35 mL of DI Water to form a homogenous solution and kept under vigorous magnetic stirring at room temperature. To that, 1.65 mL of hydrazine hydrate (85%, w/w %) and 3.35 mL of aqueous ammonia solution were added. The mixture was transferred to a 50 mL Teflon vessel held inside a stainless steel autoclave, closed and placed in a preheated oven at 180 ^oC for 4 hours. A dark-blue coloured solution was collected in a beaker. For galvanic replacement, top 20 ml of Te NWs (0.217 mmol) solution was precipitated with acetone, and redispersed in 50 ml water. 92 mg of $PdCl_2$ (0.521 mmol) was dissolved in 2 ml conc. HCl followed by 50 ml water and was added into the previous Te nanowires solution and the reaction mixture was kept in an incubator shaker at 30 ^oC for 12 h at 100 rpm. Finally, product was collected by centrifugation (12,000 rpm, 10 min). The product was washed several times with double-distilled water and absolute ethanol, dried in oven at 70 °C and was used for further characterization and catalysis.

Materials Characterization: Powder X-ray diffraction (XRD) patterns were recorded using a Rigaku Ultima IV diffractometer with Cu Kα radiation (Cu Kα, λ = 1.5418 Å, 40 kV, and 40 mA). Field-emission scanning electron microscopy images were recorded using JEOL JSM-7600F equipped with energy-dispersive X-ray spectroscopy (EDS). TEM and HRTEM were carried out using JEOL JEM-F200 equipped with electron energy loss spectroscopy (EELS). Inductively coupled plasma mass spectrometry (ICP-OES, Perkin Elmer 700DV) was used to detect atomic ratios of various metals and several non- metals at concentrations as low as one part in 1ppm, UV–Vis absorption spectra were recorded using Agilent Cary 60-UV-Vis spectrometer at room temperature. All samples were dried under vacuum at 70 ^0C for 4 h before analysis. IR spectra were collected using Perkin Elmer FTIR spectrometer using KBr pellet. Hard X-ray photoelectron spectroscopy (HAXPES) measurements and Extended X-ray absorption fine structure (EXAFS) measurements were carried out at P-09 and P-65 beamlines, respectively, at PETRA-III research laboratory, DESY-Deutsches Elektronen-Synchrotron, Hamburg, Germany. All measurements were performed at room temperature and a photon energy of 5946 eV was used for the HAXPES experiments. For the EXAFS measurements, the incident (I0) and transmitted (It) photon intensities were recorded at the Pd K (24350 eV) edge of the sample. Fitting of the R-space experimental data to theoretical EXAFS functions was performed using various applets of Demeter Program.

Catalytic hydrogenation of 4NP by $NaBH_4$: This reaction was carried out at room temperature (27 ^oC) to examine catalytic activity of the nanowires. The reaction kinetics were monitored using UV-Vis absorbance spectroscopy. In a typical procedure, a mixture of 2.7 ml 0.1 mM 4NP and 0.3 ml 0.6 M $NaBH_4$ in DI water was taken together in a quartz cuvette. Large excess of the reducing agent was taken to confirm pseudo first order nature of the reaction. 0.3 mg of catalyst dispersion in water was added to it and absorbance values were collected at regular time intervals. For recyclability study, the catalyst was recovered first by centrifugation and used without further cleaning. The process was repeated. The concentrations of 4NP were calculated by using Lambert Beer's Law and rate constant for each cycle was calculated.

Fabrication of column reactor and catalysis: 5 mg of Pd NWs was dispersed in 5 ml of ethanol by sonication for 5 min at room temperature. Whatman-42 filter paper each of 3 cm in diameter was circularly cut and then the catalyst ink was carefully and homogenously drop-casted onto the filter paper. It was allowed to dry naturally and stacked together inside a plastic cylinder, to make the lab scale flow reactor. The product was collected at the bottom using a funnel. In each slot, 3 ml of reactant mixture (2.7 ml 0.1 mM 4NP and 0.3 ml 0.6 M $NaBH_4$ in DI water) was poured in to flow reactor at a rate of 6 ml/min and the product UV was recorded each time to confirm the complete conversion. The reaction was also carried out with high concentration of reactants. For catalyst activity regeneration 70 ml hot water poured on the catalyst bed after every 10 cycles.

ATR IR measurements: In-situ FTIR measurements were recorded using Bruker Alpha-ATR-FT-IR spectrometer. For individual components, FTIR spectra were recorded in liquid form with water as background. The sample conc. were optimized to obtain the interpretable IR signal. To follow the catalytic reaction, FTIR spectra were recorded for 12 µl of 0.13 M 4NP followed by addition of 10 µl of 2.4 M $NaBH_4$. After addition of 10 µl of catalyst dispersion (3 mg Pd NWs in 1 ml water) to the above reaction mixture, FTIR spectra were continuously recorded to examine the changes happening during catalysis. Note that water evaporates during the reaction and each time, water content in the total sample was optimized to maintain steady background signal.

Conflicts of interest

There are no conflicts to declare.

Acknowledgements

UKG thanks Department of Science & Technology (DST), Govt. of India for Ramanujan Fellowship. LS thank UGC for the research fellowship. The SEM, XRD facilities at IISER Mohali are

gratefully acknowledged. The authors thank Manjeet Chhetri and Pramod Patil for their help with experiments and useful discussions. Portions of this research were carried out at the light source PETRA III of DESY, a member of the Helmholtz Association (HGF). We would like to thank Edmund Welter for assistance at beamline P-65. Financial support by the DST, India provided within the framework of the India@DESY collaboration is gratefully acknowledged.

References

1. L. L. Chng, N. Erathodiyil and J. Y. Ying, *Acc. Chem. Res.*, 2013, **46**, 1825-1837.

2. A. Bej, K. Ghosh, A. Sarkar and D. W. Knight, *RSC Adv.*, 2016, **6**, 11446-11453.

3. G. Zheng, K. Kaefer, S. Mourdikoudis, L. Polavarapu, B. N. Vaz, S. E. Cartmell, A. Bouleghlimat, N. J. Buurma, L. Yate, A. R. de Lera, L. M. Liz-Marzan, I. Pastoriza-Santos and J Perez-Juste, *J. Phys. Chem. Lett.*, 2015, **6**, 230-238.

4. O. M. Wilson, M. R. Knecht, J. C. Garcia-Martinez, R. M. Crooks, *J. Am. Chem. Soc.*, 2006, **128**, 4510-4511.

5. Y. Li, Hong, D. M. Collard and El-Sayed, *Org. Lett.*, 2000, **2**, 2385-2388.

6. M. J. Perez-Lorenzo,*J. Phys. Chem. Lett.*, 2012, **3**, 167-174.

7. S.-i. Yamamoto, H. Kinoshita, H. Hashimoto, Y. Nishina, *Nanoscale* 2014, **6**, 6501.

8. X. Gu, W. Qi, X. Xu, Z. Sun, L. Zhang, W. Liu, X. Pan, D. Su, *Nanoscale* 2014, **6**, 6609.

9. J. Liu, G. Hu, Y. Yang, H. Zhang, W. Zuo, W. Liu, B. Wang, *Nanoscale* 2016, **8**, 2787.

10. M. Zhao, L. Sun and R. M. Crooks, *J. Am. Chem. Soc.*, 1998, **120**, 4877-4878.

11. S. Bolisetty, M. Arcari, J. Adamcik and R. Mezzenga, *Langmuir*, 2015, **31**, 13867-13873.

12. A. K. Srivastava, K. Mondal, K. Mukhopadhyay, N. E. Prasad and A. Sharma, *RSC Adv.*, 2016, **6**, 113981-113990.

13. J. Wang, Z. Wu, T. Li, J. Ye, L. Shen, Z. She andF. Liu, *Chem. Eng. J.*, 2018, **334**, 579-586.

14. X. Liu, Y. Li, Z. Xing, X. Zhao, N. Liu and F. Chen, *New J. Chem.*, 2017, **41**, 15027-15032.

15. H. Koga, N. Namba, T. Takahashi, M. Nogi and Y. Nishina, *ChemSusChem* 2017, **10**, 2560-2565.

16. H. Miyamura, R. Matsubara, Y. Miyazaki and S. Kobayashi, *Angew. Chem. Int. Ed.* 2007, **46**, 4151-4154.

17. S. Kanaoka, N. Yagi, Y. Fukuyama, S. Aoshima, H. Tsunoyama, T. Tsukuda and H. Sakurai, *J. Am. Chem. Soc.* 2007, **129**, 12060-12061.

18. B. Yang, C. Zhao, M. Xiao, F. Wang, C. Li, J. Wang and J. C. Yu, *Small*, 2012, **9**, 1003-1007.

19. J. Liu, K. He, W. Wu, T.-B. Song, M. G. Kanatzidis, *J. Am. Chem. Soc.*, 2017, **139**, 2900-2903.

20. Y. Chen, G. C. Egan, J. Wan, S. Zhu, R. J. Jacob, W. Zhou, J. Dai, Y. Wang, V. A. Danner, Y. Yao, K. Fu, Y. Wang, W. Bao, T. Li, M. R. Zachariah and L. Hu, *Nat. Commun.*, 2016, **7**, 12332.

21. X. S. Zhao, X. Y. Bao, W. Guo and F. Y. Lee, *Mater. Today*, 2006, **9**, 32-39.

22. P. Djinovic, I. G. O. Crnivec, B. Erjavec and A. Pintar, *Appl. Catal. B.*, 2012, **125**, 259-270.

23. H. Jiao, Zhao, X. Lv, C.; Y. Wang, D. Yang, Z. Li and X. Yao, *Sci. Rep.* , 2016, **6**, 34068.

24. Y. Wang, L. Zhu, L. Zong, X. Yan and Li, *ACS Sustain. Chem. Eng.*, 2017, **5**, 10673-10681.

25. S. Ma, X. Chen, B. Zhao, H. Dong, Q. Yuan, L. Li, J. Lv, L. Shi and L. Chen, *Appl. Catal. A.*, 2017, **536**, 35-44.

26. Y. Liu, Y. Zheng, B. Du, R. R. Nasaruddin, T. Chen and J. Xie, *Ind. Eng. Chem. Res.* 2017, **56**, 2999-3007.

27. J. He, W. Ji, L. Yao, Y. Wang, B. Khezri, R. D. Webster and H. Chen, *Adv. Mater.*, 2014, **26**, 4151-4155.

28. E. Menumerov, K. D. Gilroy, M. Hajfathalian, C. J. Murphy, E. R. McKenzie and R. A. Hughes, Neretina, *Catal. Sci. Technol.*, 2016, **6**, 5737-5745.

29. M. Rana, P. K. Patil, M. Chhetri, K. Dileep, R. Datta and U. K. Gautam, *J. Colloid Interface Sci.*, 2015, **463**, 99-106.

30. Z. Dong, X. Le, X. Li, W. Zhang, C. Dong and J. Ma, *Appl. Catal. B.*, 2014, **158-159**, 129-135.

31. X. Huang and N. Zheng, *J. Am. Chem. Soc.*, 2009, **131**, 4602-4603.

32. W. Hong, C. Shang, J. Wang and E. Wang, *Energy Environ. Sci.*, 2015, **8**, 2910-2915.

33. J. Kye, M. Shin, B. Lim, J.-W. Jang, I. Oh and S. Hwang, *ACS Nano*, 2013, **7**, 6017-6023.

34. S. Y. Sayed, F. Wang, M. Malac, A. Meldrum, R. F. Egerton and J. M. Buriak, *ACS Nano*, 2009, **3**, 2809-2817.

35. M. Sun, Y. He, W. Yang and M. Yin, *Soft Matter*, 2014, **10**, 3426-3431.

36. H.-W. Liang, S. Liu, J.-Y. Gong, S.-B. Wang, L. Wang and S.-H. Yu, *Adv. Mater.*, 2009, **21**, 1850-1854.

37. H.-H. Li, S.-Y. Ma, Q.-Q. Fu, X.-J. Liu, L. Wu and S.-H. Yu, *J. Am. Chem. Soc.*, 2015, **137**, 7862-7868.

38. D. Wen, S. Guo, S. Dong and E. Wang, *Biosens. Bioelectron.*, 2010, **26**, 1056-1061.

39. H. Tao, X. Sun, S. Back, Z. Han, Q. Zhu, A. Robertson, T. Ma, Q. Fan, B. Han, Y. Jung and Z. Sun, *Chem. Sci*, 2018, **9**, 483-487.

40. Y. Sun, A. I. Frenkel, R. Isseroff, C. Shonbrun, M. Forman, K. Shin, T. Koga, Y. White, M. H. Rafailovich and J. C. Sokolov, *Langmuir*, 2006, **22**, 807-816.

41. V. V. Srabionyan, A. L. Bugaev, V. V. Pryadchenko, L. A. Avakyan, J. A. van Bokhoven and L. A Bugaev, *J. Phys. Chem. Solids*, 2014, **75**, 470-476.

42. P. Tian, X. Xu, C. Ao, R. Si, W. Tu, J. Xu and Y.-F. Han, *ChemSusChem*, **2017**, *10*, 3342-3346.

43. N. Pradhan, A. Pal and T. Pal, *Langmuir*, 2001, **17**, 1800-1802.

44. S. Wunder, F. Polzer, Y. Lu and Y. Mei, *J. Phys. Chem. C,* 2010, **114**, 8814-8820.

45. K. Ghosh, S. M. Mandal, S. Kundu, S. Nath and T. Pal, *Appl. Catal. A.*, 2004, **268**, 61-66.

46. C. Avelino, C. N. Patricia and S. Pedro, *Angew. Chem. Int. Ed.*, 2007, **46**, 7266-7269.

47. F. Visentin, G. Puxty and O. M. Kut, K Hungerbühler, *Ind. Eng. Chem. Res.* 2006, **45**, 4544-4553.

48. D.-W. Zhuang, H.-B. Dai and P. Wang, *RSC Adv.*, 2013, **3**, 23810-23815.

49. A. Patel and R. Dawson, *Hydrometallurgy*, 2015, **157**, 219-225.

50. A. Gloskovskii, G. Stryganyuk, G. H. Fecher, C. Felser, S. Thiess, H. Schulz-Ritter, W. Drube, G. Berner, M. Sing, R. Claessen and M. Yamamoto, *J. Electron. Spectrosc. Relat. Phenom.,* 2012, **185**, 47-52.

51. B. Ravel and M. Newville, *J. Synchrotron Radiat.*, 2005, **12**, 537-541.

